



Calhoun: The NPS Institutional Archive
DSpace Repository

Faculty and Researchers

Faculty and Researchers' Publications

1991

Attitude control of flexible communications satellites

Agrawal, Brij N.; Gran, Richard

Monterey, California. Naval Postgraduate School

<https://hdl.handle.net/10945/36463>

This publication is a work of the U.S. Government as defined in Title 17, United States Code, Section 101. Copyright protection is not available for this work in the United States.

Downloaded from NPS Archive: Calhoun



Calhoun is the Naval Postgraduate School's public access digital repository for research materials and institutional publications created by the NPS community. Calhoun is named for Professor of Mathematics Guy K. Calhoun, NPS's first appointed -- and published -- scholarly author.

Dudley Knox Library / Naval Postgraduate School
411 Dyer Road / 1 University Circle
Monterey, California USA 93943

<http://www.nps.edu/library>

ATTITUDE CONTROL OF FLEXIBLE COMMUNICATIONS SATELLITES

Brij N. Agrawal*
 Naval Postgraduate School
 Monterey, California 93940

Richard Gran†
 Grumman Aerospace Corporation
 Bethpage, New York 11714

Abstract

This paper investigates alternate control techniques for the attitude control of a three axis stabilized flexible communications satellite consisting of a large reflector and a solar array. The control configurations consisted of three classes: Class 1 - sensors and actuators co-located on the central body, Class 2 - actuator on the central body and sensors distributed, and Class 3 -actuators and sensors distributed. Criteria are developed for modal truncation. The results indicate that Class 2 can cause instability and is not generally a desirable design approach. An experimental setup to study the effects of flexibility on attitude control performance during slew maneuvers and wheel desaturation is also discussed.

I. Introduction

The current trend in the design of communications satellites has been towards higher electric power and narrower antenna beam-width in order to reduce the size of ground station antennas. This trend in the design results in lower structural frequencies due to larger solar arrays and antenna reflectors. The decrease in the beamwidth calls for higher pointing accuracy which in turn calls for higher closed-loop bandwidth. Therefore, the current trend in the design of communications satellites results in some structural frequencies within control bandwidth, resulting in the potential for controllability interactions. Attitude control design for such spacecraft becomes a challenging problem. In the past decade, several new control techniques have been proposed for large flexible structures. The application practicality of these techniques for communications satellites, however, requires further work.

At INTELSAT, a study was undertaken to investigate analytically alternate techniques for attitude control of three-axis stabilized flexible spacecraft. At the Naval Postgraduate School, an experimental set-up has been developed to experimentally investigate alternate control techniques for flexible spacecraft. This paper presents the results of this work.

II. Spacecraft Configuration

The spacecraft configuration used for the study^{1,2,3} is shown in Fig. 1. It is a three-axis-stabilized spacecraft. It consists of a central body which is assumed to be rigid. Attached to it are two flexible structures: one is a 10 m diameter deployable antenna reflector supported by two Astromast structures and the other is a solar array. A smaller antenna, 3 m diameter, is modeled as a

concentrated mass. The feed of the 10 m diameter reflector is attached to the central body. The performance is measured by the pointing error of the reflector, resulting in beam pointing error, and the distance between the feed and the reflector, resulting in defocusing of the beam.

The three classes of control systems were investigated during the study.

Class 1 - actuators and sensors co-located at the central body

Class 2 - actuators at the central body but sensors at the central body and at the antenna

Class 3 - actuators and sensors distributed on the spacecraft so that the antennas may be controlled independent of the central body

The available actuators are three reaction wheels at the central body, a two-degree-of-freedom gimbal drive for the larger reflector, and a tension drive that applies a force between the centers of the astromasts that hold the reflector. The available sensors are to measure attitude and rates for the central body and the larger reflector, and the distance from the feed horn to the antenna reflector.

The major disturbances on the satellite are the solar array torques due to solar pressure, thruster torques, and white disturbance noise associated with the actuators.

III. Analytical Simulation

A finite element model of the spacecraft was developed using NASTRAN. Table 1 gives natural frequencies for the structural modes. The structural modes can be divided into four categories: uncontrollable modes, unobservable modes, stable interacting modes, and unstable interacting modes. Uncontrollable modes are not excited by any of the actuators. Unobservable modes are not sensed by any of the sensors. Stable interacting modes are both controllable and observable at the actuator/sensor locations with the identical mode characteristics at each location (the same slope for rotational actuating/sensing). Unstable interacting modes are both controllable and observable at the actuator/sensor locations with mode characteristics that are of the opposite sign. As an example, Fig. 2 shows categorization of some of the structural modes.

The first step in the design of the control system is the determination of which of the modes are significant. Since antenna pointing is a critical performance parameter, it must be used in evaluating the importance of any mode. Thus, the modes that are kept in the synthesis model are (a) the modes which are controllable and/or observable and which have the largest effect on antenna pointing and (b) the modes which are unstably interacting, even though they may

*Professor, Department of Aeronautics and Astronautics
 Associate Fellow
 †Director of Advanced Concepts

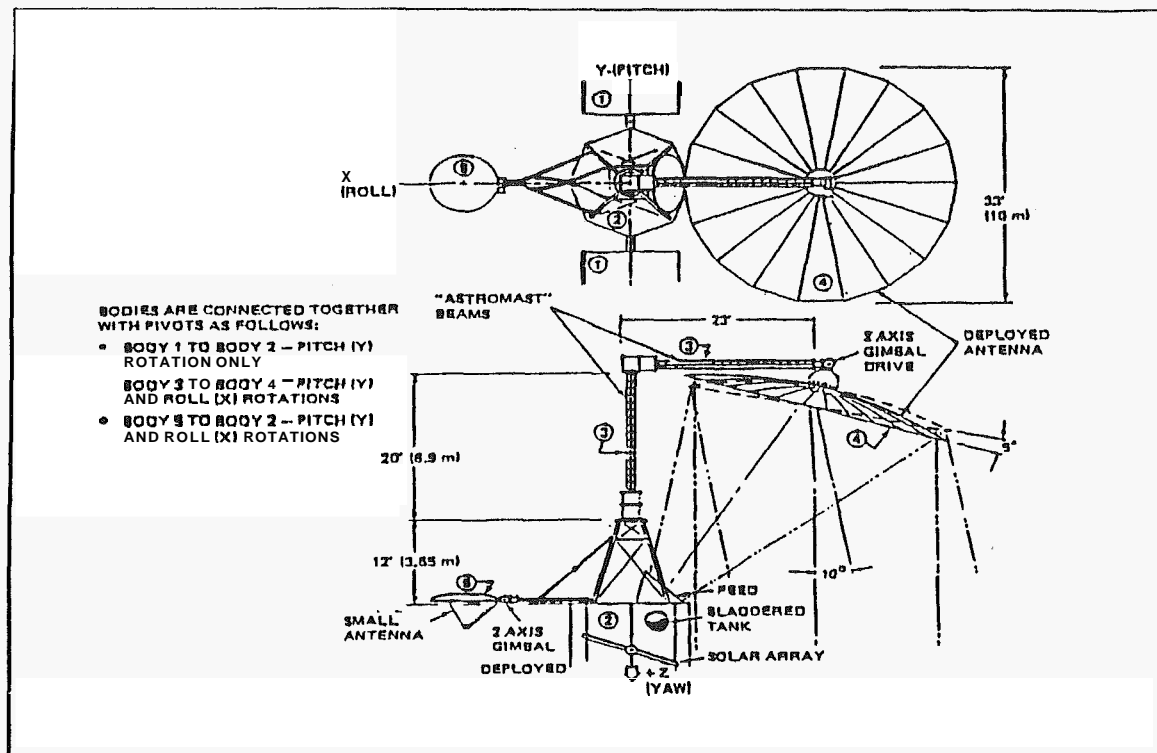
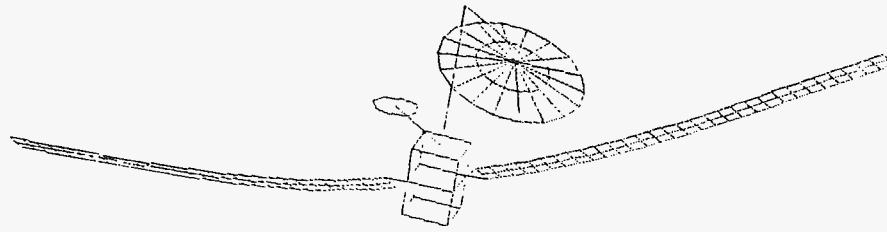


Figure 1. Spacecraft Configuration

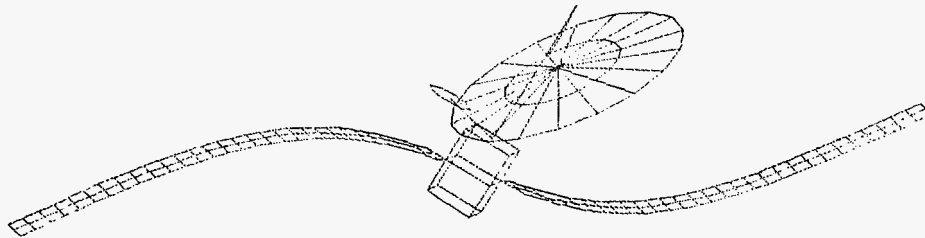
Table 1. Natural Frequencies and Mode Shapes

Mode	Frequency, <i>tit</i>	G.M., $\text{kg} \times 10^{-3}$	Description
1-6	0		Rigid Body Modes
7	.0589	.0900	Solar array - 1st rym bending
8	.0619	.0256	Large antenna - 1st lateral trans
9	.1329	0.107	Large antenna 5 solar array - pitch
10	.1346	.00885	Large antenna - roll
11	.1361	.1843	Solar array - 1st anti-torsion
12	.1368	.0614	Large antenna pitch - sol array 5 1st sym torsion
13	.1791	.1096	Solar array - 1st anti-bending-ant roll
14	.2205	.0268	Large antenna pitch 5 lat trans
15	.3528	.0009	Solar array - 2nd sym bending
16	.4465	.0033	Solar array - 2nd anti bending
17	.5747	.0992	Solar array - 2nd anti-torsion
18	.5747	.0991	Solar array - 2nd rym torsion
19	.7362	.1046	Solar array - 1st In-plane bending
20	.7668	.0367	Astro mast handing - spacecraft roll
21	.9694	.0908	Solar array - 3rd sym bend
22	1.152	.0498	Solar array - 3rd anti-bend
23	1.188	.0609	Astro mast bending - spacecraft pitch
24	1.224	.0679	Solar array - 3rd anti-torsion
25	1.224	.0684	Solar array - 3rd sym torsion
26	1.375	.0320	Astro mast bending - spacecraft roll
27	1.885	.0920	Solar array - 4th bend
28	2.055	.1030	Solar array - 4th anti bend
29	2.130	.0569	Solar array - 4th anti torsion
30	2.130	.0568	Solar array - 4th sym torsion
31	3.000	.1086	Solar array - anti-In-plane bending

1908-027P



a) Mode 7, Frequency 0.058 unobservable at core and antenna, uncontrollable by torquer at core and at antenna.



b) Mode 13, Frequency 0.179 Hz observable, controllable, and unstably interacting for any sensor not at core mass,

Figure 2. Spacecraft Structural Modes

Table 2. Observability and Controllability of Structural Modes

Mode No.	Observability		Stable or unstable at		Retain R or Discard D		
	No	Yes	Solar Array	Antenna	Class 1	Class 2	Class 3
1	✓				D	D	D
8	At Core	At Antenna			D	n	n
9	At Core	At Antenna			D	n	n
10	At Core	At Antenna			D	R	n
11	J				D	D	D
12	✓				D	D	D
13		✓	U	U	n	n	n
14		✓	2	S	n	n	n
15	✓				D	D	D
16		✓	S	U	n	n	n
17	✓				D	D	D
18	✓				D	D	D
19	✓				D	D	D
20		J	S	U	n	n	n
21	J				D	D	D
22		✓	U	U	n	n	n
23		✓	3	U	n	n	R
24	✓				D	D	D
25	J				D	D	D
26		J	U	S	n	n	n
27	✓				D	D	D
28		J	S	S	n	n	n
29	J				D	D	D
30	✓				D	D	D
31		✓	S	U	n	n	n

NOTES:
 1 For attitude sensor located in center body, nodes 400 through 410
 2 Will not excite solar array
 3 Neutral because control torque is uniformly distributed on solar array about Y axis

08-028P

not effect antenna pointing.

Next, the rigid body bandwidth required to achieve the desired pointing accuracy using the disturbance torques is determined. For the structural modes with 0.1% damping, it is desirable to retain modes with natural frequencies up to 100 times the closed loop bandwidth. The controller design and the number of modes retained is iterated if the bandwidth becomes larger. Table 2 gives the observability and stability of structural modes and identifies whether a mode is retained or discarded.

It was found to be necessary to include actuator and sensor dynamics in control design. They can have destabilizing effect on the control system because of the phase shift included. In addition, the sensor noises are critical for proper determination of gains. The pointing errors can be normally minimized by selecting a high gain but since high gain amplifies sensor noise, there is a "best" gain to minimize pointing error.

The reduced state feedback control design algorithm developed by Rossi⁴ was used to determine feedback gains. If the designed control system is structured as shown in Fig. 3, then the algorithm can be used to determine the feedback and feed forward gains that optimize the performance index.

$$J = \int_0^{\infty} (Z^T Q_z Z + u^T R u) dt \quad (1)$$

where

Z is the output (which is not necessarily the sensor)
 u is the control
 Q_z is the weight on the output
 R is the weight on the control

The block diagram shown in Fig. 3 is structured so that the optimal design that results from minimizing performance index simultaneously gives the best feedback gain K_f and the best compensation system. The compensator that results is of order m, where m is the number of integrators in the compensator at the bottom of Fig. 3. The optimal control develops the control signal u_1 (the input to the actuators) and the control u_2 (the input to the compensator integrals) so that the resulting feedback gains will be the $K_{z1}, K_{z2}, \dots, K_z$ which directly determine the compensator zeros (the K_{z1} are the coefficients of the numerator transfer function matrix), and $K_{p1}, K_{p2}, \dots, K_{pm+1}$, which directly determine the poles of the compensator. The minimization of performance index is with respect to the three sets of gains K_f , K_z , and K_p . For this design, the output Z is a measure of the performance of the spacecraft, namely the pointing error of the antenna.

The weighting matrices Q and R in Eq. (1) are used to adjust the relative amount of control authority used. This is not important for the control u_1 , which is the compensator input, since this control does not have any saturation constraint, but the control u_2 , which drives the actuators, must be limited since the actuators have a maximum amount of control authority (reaction wheels cannot torque the vehicle when the motor speed reaches its maximum).

The reduced state algorithm gives a solution which depends on the initial conditions. The minimizing feedback gain is determined from a search. The algorithm for determining the minimum uses an explicit calculation of the gradient and Hessian tensors for J, and the search is done in four steps. The first step is to compute the gradient and Hessian matrices and then to diagonalize the Hessian. Since the

Hessian is symmetric, the diagonalization can be performed by an orthogonal transformation. In general the Hessian will not be positive definite; therefore, the negative eigenvalues are arbitrarily changed in sign to make the step direction correspond to a locally quadratic curve fit. Thus if H_0 represents the Hessian matrix at the zeroth iteration, this step consists of forming the following matrices:

$$H_0 = [V_1 V_2] \begin{bmatrix} D_1 & 0 \\ 0 & -D_2 \end{bmatrix} \begin{bmatrix} V_1^T \\ V_2^T \end{bmatrix} \quad (2)$$

where

$D_{1,2}$ are diagonal matrices with positive entries
 $V_{1,2}$ are the elements of the orthogonal transformation

and

$$H^t = [V_1 V_2] \begin{bmatrix} D_1 & 0 \\ 0 & D_2 \end{bmatrix} \begin{bmatrix} V_1^T \\ V_2^T \end{bmatrix} \quad (3)$$

The only difference between Eq. (2) and Eq. (3) is that H^t in Eq. (3) is now positive definite.

The second part of the algorithm is the determination of the step direction for search. This is done by using the Taylor series for the cost as follows:

$$J(K_1) = J(K_0) + (K_1 - K_0)^T G + Q(K_1, K_0, H) + \dots \quad (4)$$

where Q is the quadratic term in the Hessian H
 K is the vector of gains that are being optimized
 G is the gradient (in this case a vector)

The third part of the algorithm is the determination of this step from the approximate Hessian. From Eq. (4) the step direction is given by $-(H^t)^{-1}G$. The fourth step before the process is repeated again is the determination of the step magnitude. This is accomplished using a one dimensional optimization so that $K_1 = K_0 + (a)s_0$, where s_0 is the step direction determined above and "a" is the parameter that is to be determined by the one dimensional search so that J is minimized. The use of full state optimal solution gives a lower band on J and thereby on "a". One of the important aspects of the algorithm is that its value is never permitted to cause the gains to result in an unstable solution. This is done by altering the one dimensional search if the step size is too big. Stability is tested as a by product of the gradient and Hessian calculations. The most interesting aspect of the optimization algorithm is the fact that the gradient and Hessian are developed from the same equations. These are Lyapunov type equations and are therefore solved using the same algorithm.

The overall algorithm flow is shown in Fig. 4. The program is referred to as SLOCOP. In practice we find that the solutions obtained from the reduced state feedback control designs are within 1 or 2% of the full state designs with orders of magnitude fewer gains. The important features of this design approach are that it allows one to incorporate the actuator dynamics and sensor dynamics, the noises on both the sensor and the disturbances exciting the structure, and the specifications in terms of a pre-specified model. If the latter is used, the model states are included in the dynamic description of the system (in the A matrix, the B matrix, and the measurement matrix) and are used to define the errors that are

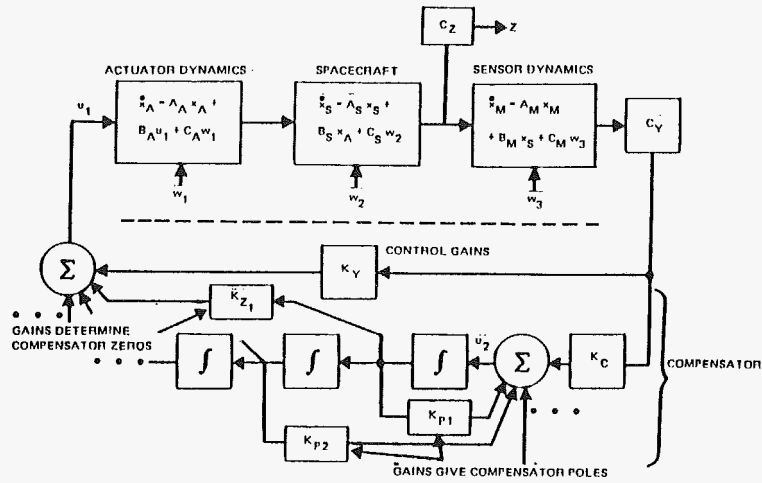


Figure 3. Reduced State Feedback Control Design

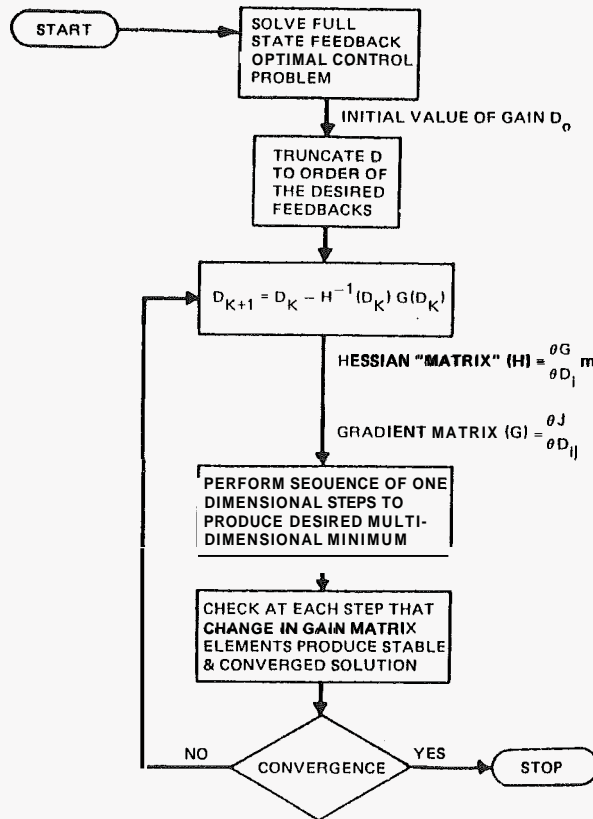


Figure 4. Constrained Optimal Control Algorithm

optimized in the performance index, but the feedback gains from the model states are not used. The last feature that is important is the explicit incorporation of the compensator dynamics. Fig. 3 shows the way the compensator dynamics are included when it is desired to design a notch filter for removing the influence of unstably interacting modes.

In the design that we developed for the antenna pointing control, we did not use a compensator. The logic behind this approach is as follows:

- (1) Determine the actuator and sensor configuration that makes the most sense so that an uncoupled design with as few gains as possible will result.
- (2) Develop a design that uses only feedback gains with no compensator and no cross feeds between individual actuators.
- (3) If, and only if, the design of (2) is not adequate, add cross feeds to determine the level of improvement that is achievable.
- (4) If, and only if, the design of (3) is not adequate, add compensation dynamics (using analysis to determine where, and how large an order, compensation is required).

The result of doing this on the spacecraft design was that we did not have to go beyond the first step. We were able to achieve pointing accuracies an order of magnitude below the desired level without compensation, and by using an extremely simple structure. The structure, shown in Fig. 5, uses feedback of the pitch roll and yaw position and rate sensors to control, the pitch roll and yaw (independently) actuators. The antenna line of sight actuator is controlled from measurements that determine the position and rate of change of the antenna to feed horn distance.

IV. Analytical Results

The Class 1 design used actuators and sensors at the central body. The six gains were computed from SLOCOP and the resulting rms antenna pointing errors were 4.6×10^{-2} , 3.3×10^{-3} , 6.6×10^{-4} deg in yaw, pitch and roll respectively, and 11.38 mm rms in defocus.

The Class 2 design used measurements at the antenna and the actuators at the central body. The attitude and rate sensors were mounted at the base of the reflector. The gains were calculated from SLOCOP and the resulting rms antenna pointing errors were 4.56×10^{-6} , 4.3×10^{-3} , 2.2×10^{-5} deg in yaw, pitch, and roll respectively, and 2.2×10^{-4} mm in defocus.

The Class 3 design used measurement at the antenna and distance between feed and antenna reflectors. The actuators are at the central body, gimbal drive for reflectors, and tension drive between astromasts. The resulting design gives rms pointing errors of 8.9×10^{-5} , 1.6×10^{-4} and 5.8×10^{-5} deg in yaw, pitch and roll respectively, and 2.2×10^{-4} mm in defocus.

It should be noted that in all three cases the designs give control that exceed 0.1 degree rms pointing requirements by at least an order of magnitude. The full state feedback solution with 180 gains gave a solution of 8.2×10^{-6} , 3×10^{-5} , and 5.5×10^{-6} rad in yaw,

pitch, and roll respectively, which is at most a factor of 10 better than the results of Class 3 with 12 gains. The nonlinear simulation code **SATSJM** was used to verify the control design results from linear analysis. Figure 6 shows attitude errors for Class 1 design. The rms pointing errors are 0.0006 deg which is better than the results from the linear analysis.

V. Experimental Simulation

At the Naval Postgraduate School, an experimental setup was developed to validate the control techniques developed for spacecraft configuration such as in Fig. 1. There were three primary design criteria for the experimental setup. First, the system should be easy to operate by graduate students without the aid of technicians. Second, it should have the ability to expand to new research areas such as space robotics and deployment of space structures. Third, the cost of the experimental setup should be within budget constraints.

Considering these design criteria, three experimental configurations were evaluated in depth: a spherical air bearing providing three-axis simulation, a disk/rod system, and pitch axis simulation on granite table with air pads. The spherical air bearing configuration was not selected mainly because of high complexity in design and operation due to gravitational effect, and cost significantly above budgetary constraints. The disk/rod system, consisting of disks connected by flexible rods, would have provided one axis simulation, been simple to operate, and would have been within budgetary constraints. This configuration was not selected because it could not be easily expanded to other areas of research. The third configuration of pitch axis simulation was selected because it met all three design criteria.

Experimental Configuration

The experimental configuration⁵ is shown in Fig. 7. The spacecraft simulator consists of a central rigid body representing the spacecraft main body, and a flexible appendage representing a reflector with a flexible support structure. The simulator is supported on air pads to reduce friction. The whole system is supported on a granite table. The central body is allowed to rotate about the vertical axis and is prevented from translational motion by an air bearing. The primary actuator is a reaction wheel located on the central body. The angular position of the central body is determined by a rotary variable differential transformer, (RVDT), and its angular rate by an angular rate sensor. Figure 8 shows the hardware of experimental setup. The fundamental cantilever frequency of the flexible structure is 0.13 Hz.

The mechanical system consists of the granite table of 1.82 m x 2.43 m x 0.267 m size and surface with a laboratory grade A 0.001" finish. The central body is 2.22 cm thick aluminum disk with a 0.76 m radius. The flexible arms are aluminum beams of 0.4 cm thickness and 2.54 cm width. The length of the first arm is 0.67 m and the length of the second is 0.61 m. The mass of each steel mass intensifier pair is 0.47 kg. Each air pad is capable of supporting 267N (60 lbf) load. The control systems consists of a VAX station 3100 Model 30, the AC-100 controller manufactured by Integrated System Inc., and associate software. The development software, which includes MATRIX_x Auto Code, Interactive Animation,¹⁸ is used to create the mathematical model and executes on the VAX station under VMS operating system. The controller has 16 channel analog input, 16 channel analog output, and 32 parallel digital input/output.

The primary actuator for the present setup is a reaction wheel. The wheel is a 0.26 m diameter, 2.22 cm thick steel dish. The motor is a DC servo motor manufactured by PMI. The motor is a

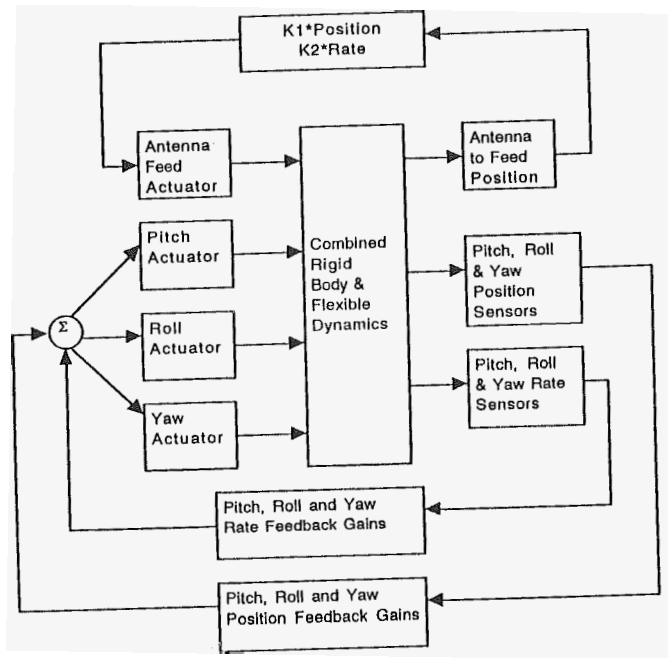


Figure 5. Block Diagram of Control System Design

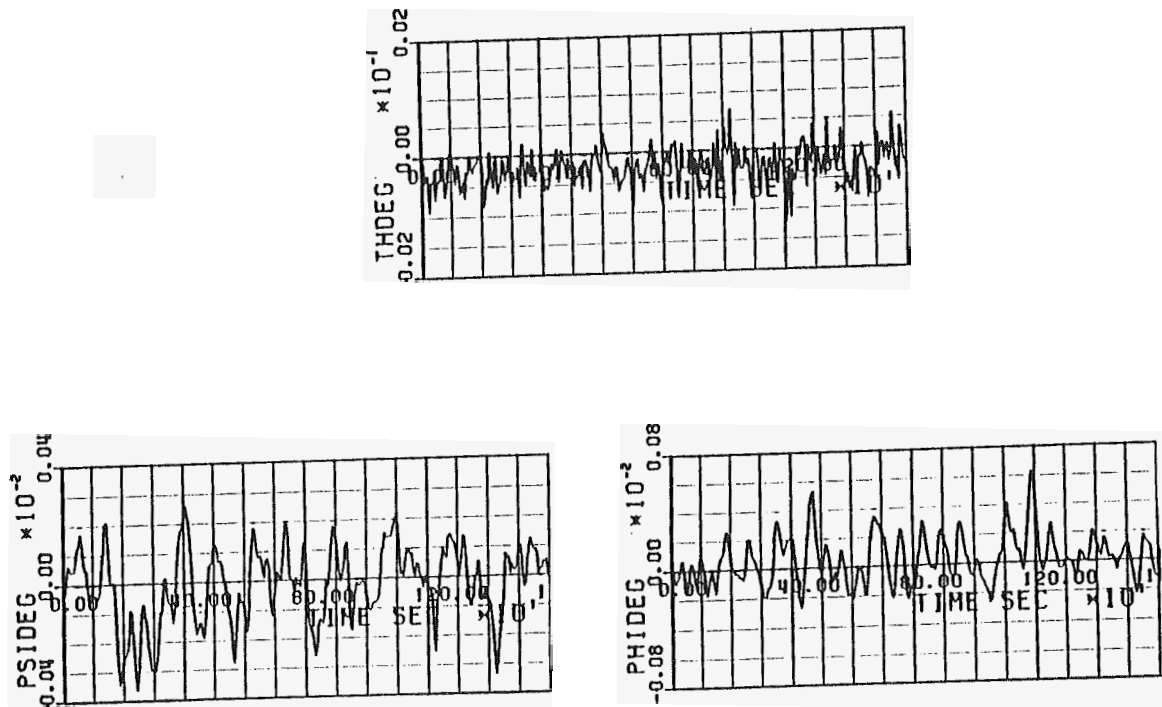


Figure 6. Nonlinear Simulations for Class 1 Control Design

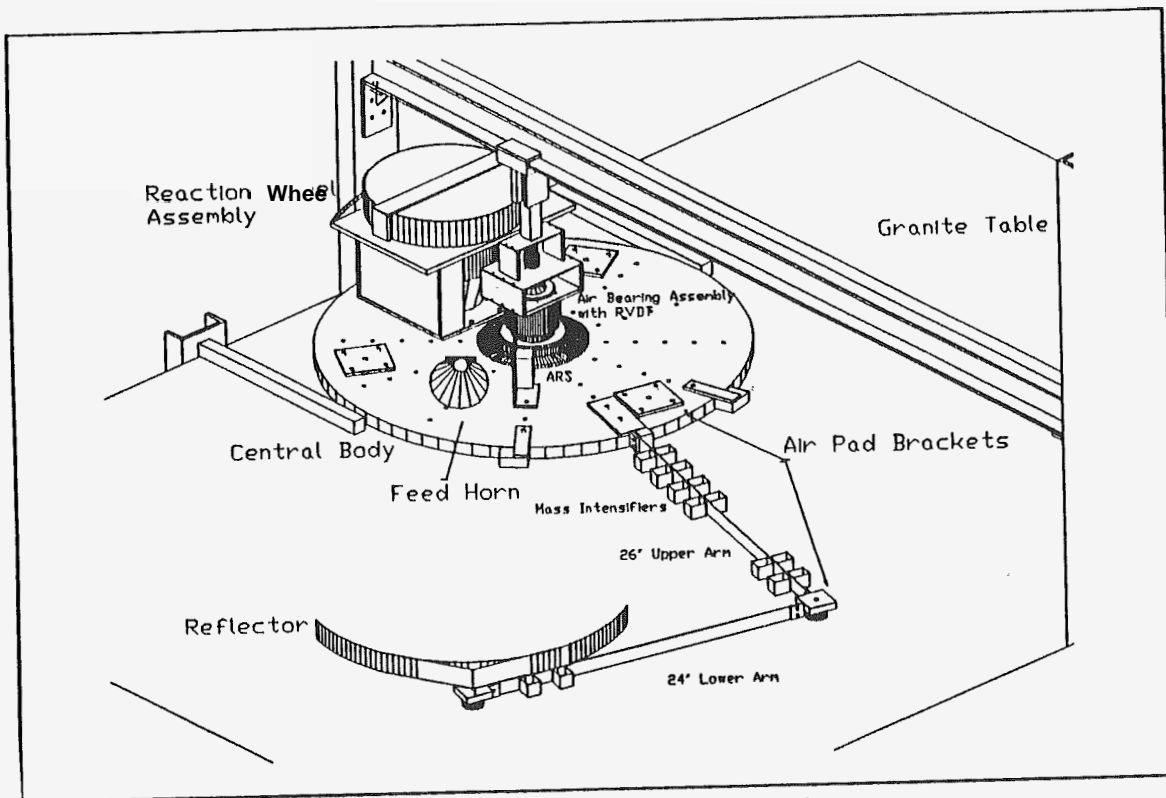


Figure 7. Experimental Set-up Configuration

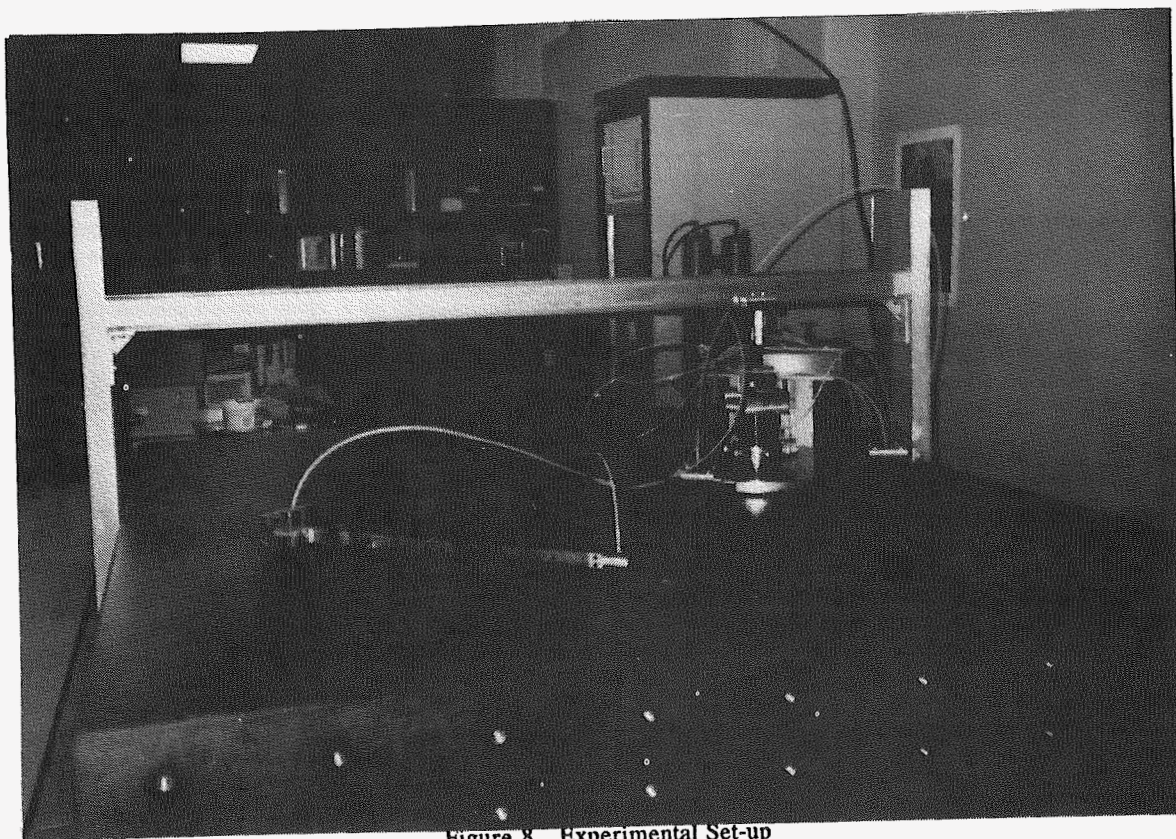


Figure 8. Experimental Set-up

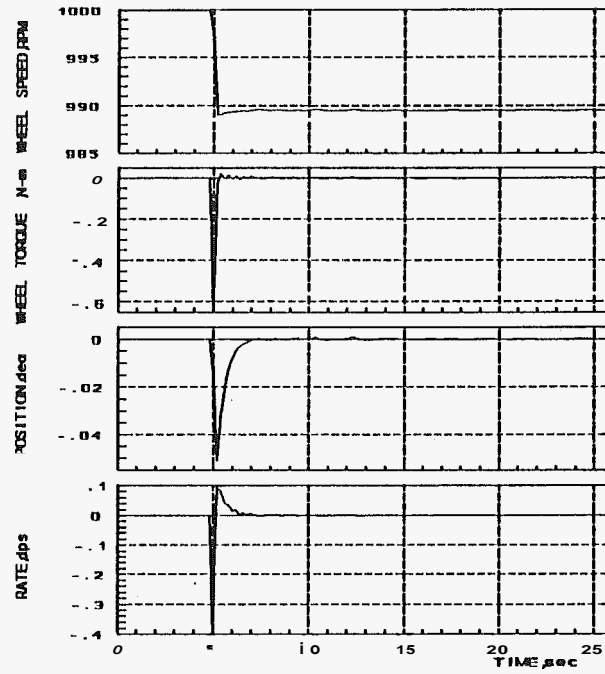


Figure 9. Central Body Response to Thruster Impulse

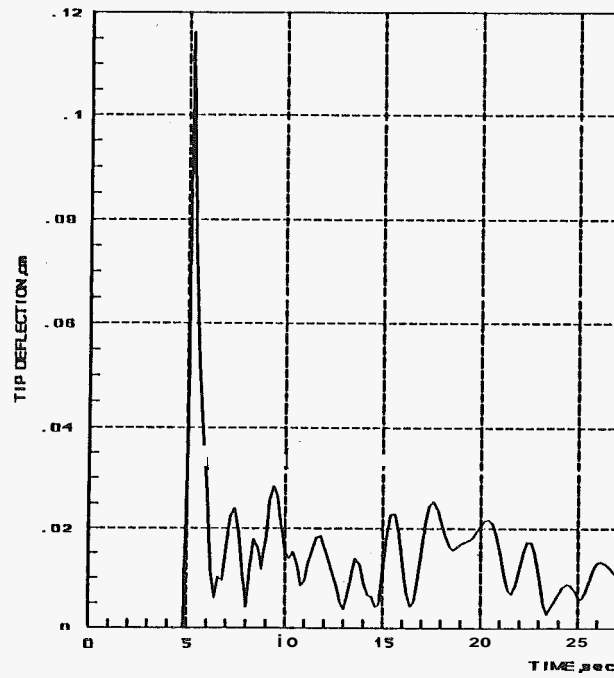


Figure 10. Tip Deflection of Flexible Arm

Model JR16M4CH with a peak torque of 37.5 N-m. The angular position of the central body is measured by a SHAEVITZ RVDT. The RVDT is a mode R30D with a range of $\pm 40^\circ$ and 0.16% linearity. The angular rate is measured by a Watson Model ARC-C121-1A ARC with a range of ± 30 deg/sec. The sensor works on the principle that the Coriolis force resulting from angular motion causes bending of the piezoelectric sensing elements.

Currently in Phase I, the experimental setup will be expanded in the future. In Phase II, piezoelectric sensors will be added on the flexible arm to provide active control. Phase III will have position sensors on the arm and a motor on the reflector support to provide angular control of the reflector. In Phase N, thrusters and liquid tanks will be added to the control body. Phase V will expand the experimental setup to include space robotics by adding motors and angular position sensors on the flexible arm joints. Phase VI will investigate the deployment of space structures.

Analytical Simulation

The equations of motion for the experimental setup are derived by using a hybrid-coordinate system, consisting of physical coordinates for the rigid body and modal coordinates for the flexible arm. The equations are:

$$I\ddot{\theta} + G + \sum_{i=1}^n D^i \dot{q}_i = T \quad (5)$$

$$\ddot{q}_i + 2\xi_i \omega_i \dot{q}_i + \omega_i^2 q_i + D^i \dot{\theta} = 0 \quad (6)$$

$$i = 1, \dots, n$$

Where I = moment of inertia of the undeformed system about rotational axis; θ = angular position of the central body; h = angular momentum of the reaction wheel; D^i = rigid-elastic coupling for the i th mode; q_i = modal coordinate for the i th mode; ξ_i = fraction of critical damping for the i th mode; ω_i = natural frequency of the i th mode; and n = number of modes kept for the analysis.

By defining the state vector in the form

$$X = [\theta, \dot{\theta}, q_1, \dot{q}_1, \dots, q_n, \dot{q}_n, h] \quad (7)$$

The second order Eqs. 6 and 7 are written in standard state variable form

$$\begin{aligned} \dot{X} &= AX + BU \\ Y &= CX \end{aligned} \quad (8)$$

where U is input vector and Y is output vector. Matrices A , B and C , completes the description of the equations in the state space form.

Analytical simulations were performed for three maneuvers: thruster impulse of 0.1 N.m.s, 5° bias maneuver, and 30° slew maneuver. For these maneuvers, both Class 1 and Class 2 control techniques were used. For Class 1, control proportional (PD) control is used by feeding back the central body angular position and angular rate for the control torque of the momentum wheel. For Class 2 control, linear-quadratic-gaussian or

LQG compensator is used. It is formed from a linear regulator and a Kalman filter estimator. The regulator design assumes full-state feedback. The MATRIX_x computer program is used for this analysis. The results from this study indicates that for thruster impulse and 5° bias maneuver Class 1 control provides acceptable performance. However, for slew maneuver, Class 2 control gives better performances. Further work is necessary to optimize the control system for slew maneuver. As an example Fig. 9 shows the response of the control system due to thruster impulse and Fig. 10 shows tip deflection of the flexible arm.

VI. Conclusions

Based on the analytical results from this study, guidelines have been developed in the attitude control design of flexible communications satellites. The structural modes that are controllable and unobservable and stably interacting are discarded. Also, the modes that stably interact are discarded if their contributions to the performance measure are small. The modes that unstably interact must always be retained. The control design must consider actuator and sensor dynamics and sensor noises. The reduced state of feedback control design algorithm provides good control performance.

For the flexible spacecraft under study, Class 1 design, which is the most robust design approach possible, satisfies the pointing requirements. Class 3 design is used to develop a fix for failure of Class 1 approach. Class 2 control design can cause stability problems and is not generally a desirable approach.

The experimental setup to validate control techniques for flexible spacecraft has been developed. The current design simulates Class 1 control where sensors and actuators are located on the central body. In the near future, it will be expanded to simulate Class 2 and Class 3 control configurations. It will be also expanded to study space robotics and deployment of space structures.

VII. References

1. Gran, R. and Proise, M., "Flexible Spacecraft Attitude Control," Final Report of INTEL-SAT Contract INTEL-064, Grumman Aerospace Corporation, Report RE-652, September 1982.
2. Singh, S.K., Gran, R. and Agrawal, B., "Comparison of Different Attitude Control Schemes For Large Communications Satellites," Proceedings of AIAA Guidance, Navigation and Control Conference, Monterey, California, August 1987.
3. Gran, R., "Finite-Dimensional Controllers For Hyperbolic Systems," Proceedings of Third VPI and SU/AIAA Symposium on Dynamics and Control of Large Flexible Spacecraft, June 1981.
4. Rossi, M., "Optimal Design of an Automatic Control System for Submerged Hydrofoil Boats," IEEE Conference on Eng. in Ocean Envs., September 1972.
5. Agrawal, B.N. and Watkins Jr., R.J., "Experimental Simulation of Attitude Control of Flexible Spacecraft," Eight VPI and SU Symposium on Dynamics and control of Large Structures, May 1991.
6. Oakley, C.M. and Canon, R.J., "Theory and Experiments in Selecting Mode shapes for Two-Link Flexible